Frederick, V. C., Ashy, T. A., Marchetti, B., Ashfold, M. N. R., & Karsili, T. N. V. (2021). Photoprotective Properties of Eumelanin: Computational Insights into the Photophysics of a Catechol:Quinone Heterodimer Model System. *Photochem*, *1*(1), 26-37. https://doi.org/10.3390/photochem1010003

photochem

MDPI

Article

Photoprotective Properties of Eumelanin: Computational Insights into the Photophysics of a Catechol:Quinone Heterodimer Model System

Victoria C. Frederick [1], Thomas A. Ashy [1], Barbara Marchetti [1], Michael N. R. Ashfold [2] and Tolga N. V. Karsili [1,*]

[1] Department of Chemistry, University of Louisiana at Lafayette, Lafayette, LA 70503, USA; victoria.frederick1@louisiana.edu (V.C.F.); thomas.ashy1@louisiana.edu (T.A.A.); barbara.marchetti1@louisiana.edu (B.M.)
[2] School of Chemistry, University of Bristol, Bristol BS8 1TS, UK; mike.ashfold@bris.ac.uk
* Correspondence: tolga.karsili@louisiana.edu

Abstract: Melanins are skin-centered molecular structures that block harmful UV radiation from the sun and help protect chromosomal DNA from UV damage. Understanding the photodynamics of the chromophores that make up eumelanin is therefore paramount. This manuscript presents a multi-reference computational study of the mechanisms responsible for the experimentally observed photostability of a melanin-relevant model heterodimer comprising a catechol (C)–benzoquinone (Q) pair. The present results validate a recently proposed photoinduced intermolecular transfer of an H atom from an OH moiety of C to a carbonyl-oxygen atom of the Q. Photoexcitation of the ground state C:Q heterodimer (which has a π-stacked "sandwich" structure) results in population of a locally excited ππ* state (on Q), which develops increasing charge-transfer (biradical) character as it evolves to a "hinged" minimum energy geometry and drives proton transfer (i.e., net H atom transfer) from C to Q. The study provides further insights into excited state decay mechanisms that could contribute to the photostability afforded by the bulk polymeric structure of eumelanin.

Keywords: photophysics; photoprotection; photostability; eumelanin; catechol; benzoquinone; ultraviolet; conical intersection

Citation: Frederick, V.C.; Ashy, T.A.; Marchetti, B.; Ashfold, M.N.R.; Karsili, T.N.V. Photoprotective Properties of Eumelanin: Computational Insights into the Photophysics of a Catechol:Quinone Heterodimer Model System. *Photochem* **2021**, *1*, 26–37. https://doi.org/10.3390/photochem1010003

Academic Editor: Marcelo I. Guzman

Received: 19 February 2021
Accepted: 7 March 2021
Published: 10 March 2021

1. Introduction

The fundamental photochemistry of prototypical organic and biological chromophores is attracting ever more attention [1–3]—driven, in part, by ambitions to advance understanding (and prevention) of photoinduced damage in biomolecules [4–11] and to improve the photoprotection offered by sunscreen molecules [12–15]. Ultraviolet (UV) excitation of any given molecule increases its total energy, typically to values in excess of many of the energy barriers associated with reaction on the ground state potential energy (PE) surface. The excited state molecules formed upon UV absorption may decay in a number of ways that have traditionally been illustrated using a Jablonski diagram. Extremes of these behaviors include:

(i) Photoreaction, by photodissociation, which constitutes the dominant decay mechanism for many small heterocyclic molecules in the gas phase. Much studied examples include phenol [2,4,16–25], pyrrole [26–34] and indole [35–38];

(ii) Photostability, wherein the photoexcited molecule decays back to the ground state, rapidly and with high efficiency, without any permanent chemical transformation. Such non-radiative decay (generically termed internal conversion) is the desired photophysical response for the DNA/RNA nucleobases [4,39–65] and, for example, for derivatives of the *p*-aminobenzoates, cinnamates, salicylates, anthranilates, camphor, dibenzoyl methanes and/or benzophenones used in commercial sunscreens [13,14]. Internal conversion processes are mediated by conical intersections (CIs) — regions of the PE surfaces where distinct

electronic states become energetically degenerate [66,67]. These points of degeneracy develop into CIs when orthogonal motions are considered, which facilitate non-adiabatic coupling (i.e., the funneling of population) from the photoexcited state to a lower (e.g., the ground) state.

Sunscreen molecules are chosen on the basis of good photostability. Those that find use in commercial sunscreen products have been chosen/engineered to absorb in the UV-A/B regions of the electromagnetic spectrum and, following photoexcitation, to undergo efficient non-radiative decay back to the ground state—releasing the excess energy as local heating in the formulation of which they are a part. In oxybenzone, for example, $\pi^*\leftarrow\pi$ excitation of the dominant (in the ground (S_0) state) enol-conformer populates the strongly absorbing $^1\pi\pi^*$ state, which relaxes—either directly or via an (optically dark) $^1n\pi^*$ state—toward its minimum energy keto-configuration (i.e., an intramolecular H atom transfer (HAT) process) and onwards towards the CI with the S_0 state at non-planar geometries (one ring twists relative to the other about the central aliphatic C–C bond). A reverse H atom transfer process on the S_0 PES and vibrational energy transfer to the surrounding solvent results in (efficient, but not complete) reformation of the original enol-conformer with a (solvent-dependent) time constant [32,68–72].

Many sunscreen molecules occur naturally on UV-exposed regions of biological systems. In mammals, for example, natural molecular sunscreens are localized in the skin (eumelanin and pheomelanin), sweat glands (urocanic acid) and the cornea of the eye (kynurenines). As with the DNA/RNA nucleobases, natural sunscreen molecules have evolved to cope with exposure to UV radiation, which, in the case of the skin, means protecting the lower epidermis from UV-induced DNA damage. Eumelanin, the most abundant melanin found in humans, provides many beneficial functions including serving as a naturally occurring sunscreen [73–75]. Eumelanin is produced via melanogenesis, wherein tyrosine is oxidized and polymerized, resulting in a heterogeneous pigment composed of cross-linked 5,6-dihydroxyindole (DHI) and 5,6-dihydroxyindole-2-carboxylic acid (DHICA) based polymers. The mechanism(s) underpinning its photostability remain active research topics, however [76–78].

Several studies have sought to address these issues by exploring aspects of the photophysics prevailing within individual molecular components of eumelanin—including DHI [79–82] and DHICA [75,83–85], various monohydroxyindoles [86,87] and catechol [88–93] in the gas and/or solution phase. Building on earlier work by Van Anh and Williams [94], Kohler and co-workers [95] recently reported ultrafast transient absorption studies following UV photoexcitation of non-covalently bonded heterodimers based on *ortho*-positioned dihydroxyphenol (catechol) and 1,2-benzoquinone groups. For experimental reasons, it was necessary to work with the chemically stable 3,5-di-*tert*-butyl substituted C and Q molecules. The experimental data provided rather convincing evidence that intermolecular HAT from the (acidic) O–H proton donor on catechol to a carbonyl oxygen (proton acceptor) group on the quinone could constitute another decay pathway and thus another source of photostability following UV photoexcitation. Here we report multi-reference computational studies designed to explore the photophysics of this model catechol (C), 1,2-benzoquinone (Q) (henceforth C:Q) heterodimer (without the *tert*-butyl substituents, for computational simplicity), which provide mechanistic insight in support of these recent experiments [95].

2. Computational Methods

The ground state minimum energy geometry of the π-stacked configuration of the C:Q heterodimer was optimized using the ωB97XD functional of Density Functional Theory [96], coupled to the 6-311+G(*d*, *p*) Pople basis set [97]. This functional was chosen since it is capable of describing the long-range correlation effects inherent to charge-separated configurations, as well as the dispersion interactions between the individual chromophores. Optimizations of other plausible side-on, hydrogen-bonded and π-stacked configurations were undertaken but, in all cases, these alternative starting structures converged to the π-stacked configuration shown below.

The present study focused on the net transfer of an H atom, so the tautomer formed by HAT was next optimized. In the closed-shell singlet configuration, this tautomer should represent an unstable high energy point on the diabatic ground state PE surface due to the long-range attractive interaction that encourages reformation of the parent heterodimer. Thus, the corresponding triplet-spin configuration of the C:Q biradical tautomer (which can also be viewed as a semiquinone, or catechoxyl, radical pair) was optimized in order to maintain a long-range minimum energy structure. A similar methodology was used recently to follow the photoinduced evolution of a cyclopropenone-containing enediyne system through to a biradical configuration [98].

Vertical excitation energies and transition dipole moments of the C:Q heterodimer were calculated using complete active space self-consistent field (CASSCF) and complete active space second-order perturbation theory (CASPT2) methods. The CASSCF calculation was state-averaged with the lowest four singlet and the lowest four triplet states and employed an active space of ten electrons in ten orbitals (10/10)—comprising the five highest valence orbitals and five lowest unoccupied molecular orbitals (shown later).

PE profiles associated with the HAT coordinate were then constructed by interpolating the geometries between the ground state minimum of the C:Q heterodimer and the biradical tautomer, using a linear interpolation in internal coordinates (LIIC). Using the CASPT2 method [99] and a cc-pVDZ basis set, PE values at each point along the LIIC were calculated for the lowest four singlet states using a state-averaged CASSCF reference wavefunction. The same (10/10) active space was used, along with an imaginary level shift of 0.5 E_H to aid convergence and circumvent the involvement of intruder states.

All DFT calculations were calculated using the Gaussian 16 computational package [100], whilst all CASPT2 calculations used the MOLPRO computational package [101].

3. Results and Discussion

An isolated gas-phase multi-reference computational study of the UV photoinduced chemistry of C:Q heterodimers is presented, the results of which support and extend conclusions reached in recent transient absorption studies of this system in a weakly interacting solvent (cyclohexane) [95]. This section is sub-divided into sections addressing the minimum energy structures of the heterodimer and its biradical tautomer, the electronic spectroscopy of the former and then the topography of the PE surfaces sampled following photoexcitation of the heterodimer.

3.1. Minimum Energy Geometries of the Ground State Heterodimer and Its Biradical Tautomer

As a reminder, the ωB97XD functional was used in order to achieve an appropriately balanced description of the dominant π-π interactions between the C and Q chromophores and the long-range correlation effects. As Figure 1a,b show, the ground state minimum energy geometry of the C:Q heterodimer exhibits a π-stacked configuration. (The Cartesian coordinates of all atoms in this minimum energy structure are provided as Supplementary Materials, as are (harmonic) normal mode wavenumbers for the ground state C:Q heterodimer and the bare C monomer.) Alternative side-on hydrogen bonding could also be expected to provide a strong intermolecular interaction, but the π-stacked ground state configuration shown in Figure 1 offers both π-π and hydrogen-bonding, and the stability of this π-stacked structure can be understood by recognizing two stabilizing interactions. One is a π–π interaction between bonding π electrons on the catechol moiety and the antibonding π* orbital localized on the benzoquinone. These orbitals are reasonably well-matched in energy. The second is the inter-chromophore hydrogen-bonding between an O–H donor, local to catechol, and a carbonyl oxygen acceptor, localized on the benzoquinone chromophore. This deduced C:Q heterodimer structure, involving one intra- and one intermolecular H-bond, is fully consistent with that derived by analysis of the Fourier transform infrared spectrum of mixed solutions of (the di-*tert*-butyl substituted forms of) C and Q in cyclohexane [95].

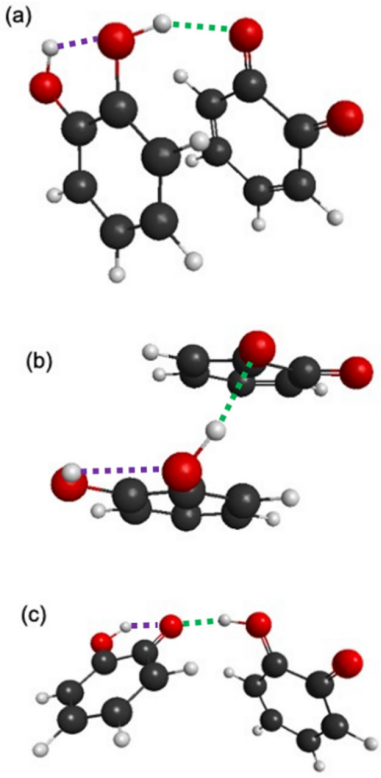

Figure 1. (**a**) Side and (**b**) top view of the optimized structure of the catechol (C), 1,2-benzoquinone (Q) (C:Q) heterodimer in its ground electronic state. (**c**) Optimized geometry of the biradical tautomer formed by H atom transfer. Intramolecular and intermolecular H-bonds are indicated by, respectively, dashed purple and green lines.

Figure 1c shows the minimum energy geometry of the biradical formed upon HAT. (The Cartesian coordinates of all atoms in this minimum energy structure are also provided in the Supplementary Materials). The "hinged" structural arrangement of the C and Q chromophores is very different from the π-stacked configuration of the ground state heterodimer, though it again displays one intermolecular and one intramolecular hydrogen bond. The breakdown of the π-stacking upon biradical formation can be understood by recognizing that the lowest energy biradical configuration has ππ* character, wherein the π- and π*-orbitals are localized on, respectively, the C and Q moieties (vide infra). The ensuing electron–electron repulsion destroys the π–π interaction inherent to the ground state parent structure, leaving inter-chromophore H-bonding as the dominant non-covalent interaction in the biradical tautomer.

We note that the experimentally studied C:Q heterodimer contains bulky *tert*-butyl substituents which may affect the π-stacking. That said, we do not expect this to have a serious impact on the excited state photophysics deduced here, as the *tert*-butyl group is a σ-perturbing substituent, while the dominant effects observed in the photophysics of C:Q are π-centered.

3.2. The Electronic Spectrum of the C:Q Heterodimer

Table 1 lists the vertical excitation energies (VEEs) to the first few singlet and triplet excited states of the C:Q heterodimer from the π-stacked minimum energy configuration. The active space orbitals used in the CASPT2 computations, shown in Figure 2, may be used along with Table 1 to identify the dominant orbital promotions involved in preparing these various excited states.

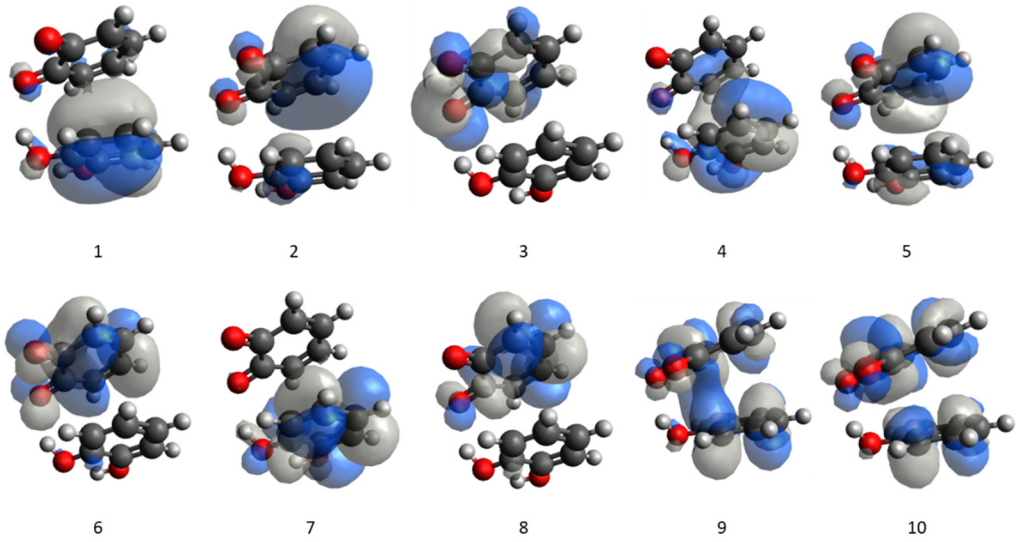

Figure 2. Active space orbitals used in the CASSCF/CASPT2 calculations of the C:Q heterodimer. Q sits above C in all depictions, but the orientation of the heterodimer structure is varied to allow better visualization of the various occupied (1–5) and virtual (6–10) orbitals. The orbital numbering aligns with that used to describe the dominant promotions associated with forming the various excited states in Table 1.

Table 1. Calculated vertical excitation energies (VEE) and oscillator strengths (*f*) to the lowest singlet and lowest triplet excited states of the C:Q heterodimer. The entries in the "Character" column show the dominant electron promotions between the active space orbitals shown in Figure 2, with the respective contributions (i.e., the squares of the associated coefficients) shown in parentheses.

Electronic State	Character	VEE/eV	*f*
S_1-S_0	6←3 (0.71) 6←3 + 6←5 (0.04)	1.93	0.001
S_2-S_0	6←5 (0.51) 6←4 (0.34)	3.23	0.0541
T_1-S_0	6←5 (0.72) 8←3 (0.04)	1.64	-
T_2-S_0	6←5 (0.73) 8←5 (0.04)	2.25	-

Vertical excitation to the S_1 state from the π-stacked ground state minimum energy geometry is dominated by electron promotion from a largely non-bonding (*n*) orbital, localized on the carbonyl oxygen atom, to an antibonding π* orbital, both of which are localized on the benzoquinone moiety. The S_1 state is best viewed as a locally excited state (i.e., the excitation is concentrated on a common chromophore) with *n*π* character, and optically "dark" (i.e., the S_1–S_0 transition has a low oscillator strength—reflecting the poor spatial overlap of the *n* and π* orbitals).

The S_2 state is best described by a mixture of two configurations. The 6←5 orbital promotion involves excitation of an electron from the π highest occupied molecular orbital (HOMO) (which is mainly localized on Q but extends over the C moiety also) to the π* lowest unoccupied molecular orbital (LUMO) localized on Q. 6←4 promotion, in contrast, involves excitation from a bonding π orbital, largely localized on the C chromophore, to the Q-localized π* antibonding orbital. Both promotions can be pictured as π*←π transitions: The S_2 state is thus best viewed as having ππ* character but, even in the vertical region, formation of the S_2 state of the heterodimer involves some electron transfer from C to Q—which likely contributes to the high oscillator strength reported in Table 1. For completeness, excitation energies to the first two triplet excited states, both of which are also best described as locally excited ππ* states, are also included in Table 1.

The predicted oscillator strengths and VEEs for the (weak) S_1–S_0 and (strong) S_2–S_0 transitions reported in Table 1 match well with the maxima evident (at λ ~595 nm and ~400 nm) in the UV absorption spectrum of the (*t*-butyl substituted) C:Q heterodimer in cyclohexane [95], lending further support to our expectation that the *tert*-butyl substituents have little effect on the electronic properties (and excited state photophysics) of the heterodimer.

3.3. Photophysics of the C:Q Heterodimer

We now consider the possible fate(s) of the C:Q heterodimer following UV photoexcitation and the potential role of such photophysics in explaining the photostability of eumelanin. Motivated by the work of Kohler and co-workers [95], the ensuing discussion focuses on the mechanism of photoinduced HAT. Figure 3a displays PE profiles of the ground and first two excited singlet electronic states along the LIIC between the ground state minimum energy geometry and that of the optimized biradical tautomer formed by HAT (henceforth Q_{LIIC})—the structures of both of which are reproduced again as insets in Figure 3a. We caution that the use of a LIIC almost inevitably means that the present calculations do not capture the true minimum energy path from reactant to product, but they are expected to identify key topographical features of the PE surfaces under study. The ground state (black) PE profile increases, reaching a maximum at Q_{LIIC} ~0.5, beyond which it decreases en route to the biradical tautomer. The electronic wavefunction of the adiabatic ground state switches at Q_{LIIC} ~0.5, as illustrated in Figure 3b,c, which illustrates the increasing $\pi\pi^*$ character of the ground state configuration of the biradical tautomer (which correlates diabatically with the S_2 state of the parent C:Q heterodimer). The stability of the biradical structure can be understood by considering the change in electronic character. In the $\pi\pi^*$ configuration, the O-atom donor of the pre-existing OH moiety contains a doubly occupied *p* orbital which, when viewed from the biradical minimum, provides a long-range repulsive interaction in the reverse HAT direction. As Figure 3b,c show, the singly occupied molecular orbitals in the S_0 state of the biradical are localized on different chromophores: the S_0 state at $Q_{LIIC} > 0.5$ is best described as a charge-separated (or charge transfer) state.

The S_1 state (red in Figure 3a) has $n\pi^*$ character in the vertical region and is bound with respect to initial motion along Q_{LIIC}—reflecting the fact that the $\pi^* \leftarrow n$ transition is localized on the benzoquinone moiety and shows no net driving force for HAT. The S_2 state, in contrast, has $\pi\pi^*$ character at the Franck–Condon geometry and shows net reactivity with respect to the "hinge-like" geometry change along Q_{LIIC}. This can be understood by recognizing that the transition involves π and π^* orbitals that are initially largely localized on a single chromophore but then develop increasing charge-separated character, as shown in Figure 3b,c. The diabatic $^1\pi\pi^*$ state progressively develops charge transfer (CT) character as $Q_{LIIC} \rightarrow 1$, which is neutralized by proton transfer from the C to the Q moiety. Such photoinduced HATs are also frequently termed proton-coupled electron transfer (PCET) or electron-driven proton transfer (EDPT) processes. Upon increasing Q_{LIIC} from the Franck–Condon region, the diabatic CT state crosses both the $^1n\pi^*$ state and the ground state. This is the origin of the evolution of the ground state electronic wavefunction described above. As in many related systems [4,102,103], these diabatic crossing points will surely be CIs when motion along orthogonal modes are considered, and represent regions of configuration space where internal conversion between electronic states is favorable (i.e., where population is funneled efficiently to the lower PE surface).

Given the foregoing descriptions of the various electronic states of the C:Q heterodimer, the reported photophysics can be rationalized as follows: Photoexcitation populates the "bright" $^1\pi\pi^*$ state, which is initially largely localized on Q but evolves spontaneously along the coordinate associated with HAT. Internal conversion is likely to occur at both the S_2/S_1 and S_1/S_0 CIs (see Figure 3a). The former may well lead to some population becoming temporarily trapped in the $^1n\pi^*$ state—as has been proposed in the case of oxybenzone [72]—while non-adiabatic interaction at the latter CI will promote efficient

internal conversion back to the S_0 state. Having accessed the S_0 PE surface, population may bifurcate to reform the ground state heterodimer (thereby demonstrating photostability) or evolve towards the biradical tautomer and thence to two (potentially harmful) semiquinone free radical species. Thus, the extent to which the C:Q heterodimer offers photoprotection and photostability will be sensitively dependent on the non-adiabatic dynamics prevailing at the S_1/S_0 CI—which will be sensitive to the detailed topography of the CI and the nuclear momenta within the evolving population. Such details, in turn, are likely to be sensitively dependent upon the natures of any (less benign than *tert*-butyl) substituents within the C and Q moieties and, in any condensed phase application, to the prevailing solvent [104]. Extrapolating to eumelanin itself, any such competition between reformation of the minimum energy ground state structure and biradical (and thence radical) formation might well be influenced by the extent (or otherwise) to which the system is able to distort away from any structural layering imposed by more extensive π-stacking between polymer strands.

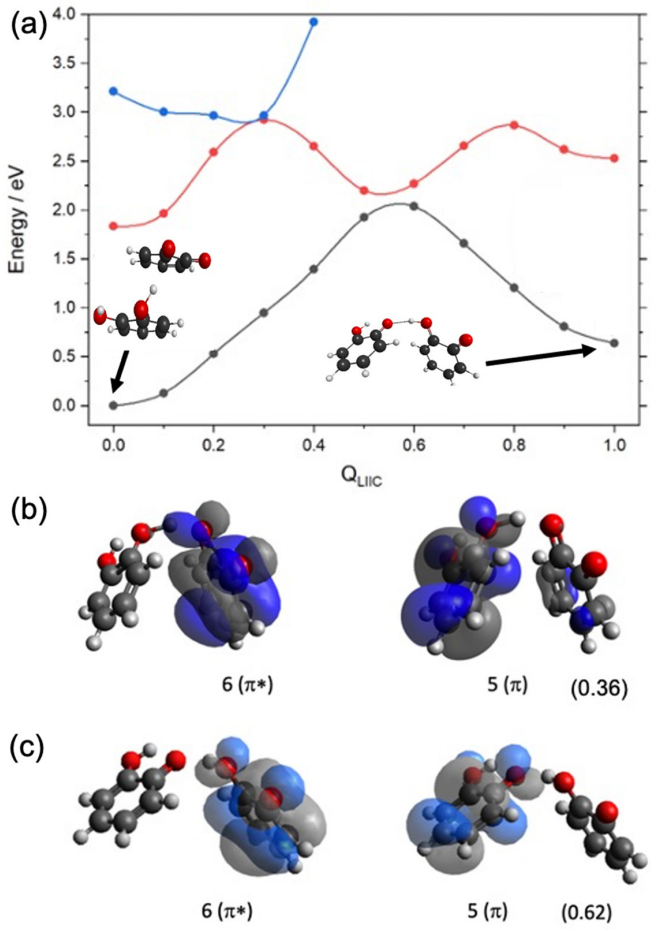

Figure 3. (**a**) Adiabatic potential energy (PE) profiles of the S_0 (black), S_1 (red) and S_2 (blue) states of the C:Q heterodimer plotted as a function of the linear interpolation in internal coordinates (LIIC) linking the ground state minimum energy geometry (at $Q_{LIIC} = 0$) with that of the optimized biradical tautomer (at $Q_{LIIC} = 1.0$). Representations of the evolving structure of the ground state heterodimer and of orbitals 5 and 6 are shown below for Q_{LIIC} = (**b**) 0.6 and (**c**) 1.0 (with, in each case, the square of the coefficient associated with this ππ* contribution to the S_0 state configuration shown in parenthesis).

4. General Discussion and Conclusions

This study, which is limited to the isolated heterodimer only, adds to the growing body of computational research aimed at exploring possible excited state decay paths in organic acid-base heterodimers. The present results support earlier suggestions, from analysis of

transient absorption measurements in a weakly interacting solvent [95], that HAT from an OH moiety of a catechol sub-unit to the carbonyl-oxygen atom of a quinone unit arranged in a π-stacked C:Q heterodimer could contribute to the pool of photoprotection mechanisms available to eumelanin upon exposure to UV radiation.

From the photophysical perspective, the π-stacked chromophores in the C:Q heterodimer exhibit similarities and differences with the excited state decay mechanisms identified for the chromophores in double-stranded DNA. UV excitation of a, base pair starts with a $\pi^*\leftarrow\pi$ promotion localized on the purine (adenine (A) or guanine (G)), which is dissipated by PCET to the pyrimidine (thymine (T) or cytosine (C)) partner and subsequent coupling via a CI to the S_0 state [105–109]. The H atom in these cases is transferred within an H-bonded base pair wherein the individual bases are parts of complementary strands (i.e., an *inter*-strand HAT process). UV photoinduced *intra*-strand electron transfer between stacked nucleobases—more reminiscent of the present situation—has been identified also, but the subsequent charge-separation (and ultimate photostability) is again achieved by an *inter*-strand proton transfer in the resulting radical anion base-pair [110,111].

As noted in the Introduction, eumelanin is a heterogeneous macromolecule, and much remains to be learned both about its exact structure and the mechanisms of the photoprotection it affords. Several studies of intramolecular processes contributing to the decay of excited states of monomers (and oligomers) of various of the proposed key sub-units of eumelanin, like DHI and DHICA, have been reported [75,82,84], along with some studies of their intermolecular interactions with solvent molecules [104]. The present work supports another inter-chromophore excited state decay pathway wherein HAT facilitates non-radiative coupling to, and reformation of, the ground state C:Q heterodimer. But, as experimental studies of (the di-*tert*-butyl substituted form of) this heterodimer also show, the biradical structure at the asymptote of the HAT coordinate can decompose to two semiquinone radicals [95]. While it is notable from an energetic perspective that absorption of one photon with an energy less than that required to break an O–H bond in bare catechol [88] could result in the formation of two semiquinone radicals, it is unlikely that nature would have adopted eumelanin as a skin pigment if such heterodimers could act as significant light-driven radical generation centers. Clearly, much further work will be needed in order to establish the importance (or otherwise) of the excited state decay pathways identified thus far for small constituent parts to the overall photoprotection afforded by bulk eumelanin.

Supplementary Materials: The following are available online at https://www.mdpi.com/2673-7256/1/1/3/s1, Cartesian coordinates associated with the various optimized structures of C:Q and (harmonic) normal mode wavenumbers for the ground states of bare C and the C:Q heterodimer.

Author Contributions: Conceptualization, T.N.V.K., B.M. and M.N.R.A.; methodology, T.N.V.K.; validation, V.C.F., B.M. and T.N.V.K.; formal analysis, V.C.F., T.A.A., B.M. and T.N.V.K.; investigation, V.C.F., T.A.A., B.M.; data curation, V.C.F., T.A.A., B.M.; writing—original draft preparation, T.N.V.K. and M.N.R.A.; writing—review and editing, T.N.V.K. and M.N.R.A.; T.N.V.K. and M.N.R.A.; project administration, T.N.V.K. and M.N.R.A. All authors have read and agreed to the published version of the manuscript.

Funding: T.N.V.K. acknowledges the University of Louisiana at Lafayette for start-up funds.

Data Availability Statement: The data supporting this study are available from the corresponding author on reasonable request.

Conflicts of Interest: The authors declare no conflict of interest.

References

1. Sobolewski, A.L.; Domcke, W.; Dedonder-Lardeux, C.; Jouvet, C. Excited-state hydrogen detachment and hydrogen transfer driven by repulsive $^1\pi\sigma^*$ states: A new paradigm for nonradiative decay in aromatic biomolecules. *Phys. Chem. Chem. Phys.* **2002**, *4*, 1093–1100. [CrossRef]
2. Ashfold, M.N.R.; King, G.A.; Murdock, D.; Nix, M.G.D.; Oliver, T.A.A.; Sage, A.G. πσ* excited states in molecular photochemistry. *Phys. Chem. Chem. Phys.* **2010**, *12*, 1218–1238. [CrossRef] [PubMed]

3. Roberts, G.M.; Stavros, V.G. The role of πσ* states in the photochemistry of heteroaromatic biomolecules and their subunits: Insights from gas-phase femtosecond spectroscopy. *Chem. Sci.* **2014**, *5*, 1698. [CrossRef]
4. Marchetti, B.; Karsili, T.N.V.; Ashfold, M.N.R.; Domcke, W. A 'bottom up', ab initio computational approach to understanding fundamental photophysical processes in nitrogen containing heterocycles, DNA bases and base pairs. *Phys. Chem. Chem. Phys.* **2016**, *18*, 20007–20027. [CrossRef] [PubMed]
5. Barbatti, M.; Aquino, A.J.A.; Szymczak, J.J.; Nachtigallová, D.; Hobza, P.; Lischka, H. Relaxation mechanisms of UV-photoexcited DNA and RNA nucleobases. *Proc. Natl. Acad. Sci. USA* **2010**, *107*, 21453–21458. [CrossRef] [PubMed]
6. Canuel, C.; Mons, M.; Piuzzi, F.; Tardivel, B.; Dimicoli, I.; Elhanine, M. Excited states dynamics of DNA and RNA bases: Characterization of a stepwise deactivation pathway in the gas phase. *J. Chem. Phys.* **2005**, *122*, 74316. [CrossRef]
7. Crespo-Hernández, C.E.; Cohen, B.; Hare, P.M.; Kohler, B. Ultrafast Excited-State Dynamics in Nucleic Acids. *Chem. Rev.* **2004**, *104*, 1977–2020. [CrossRef] [PubMed]
8. Gustavsson, T.; Improta, R.; Markovitsi, D. DNA/RNA: Building Blocks of Life under UV Irradiation. *J. Phys. Chem. Lett.* **2010**, *1*, 2025–2030. [CrossRef]
9. Middleton, C.T.; de la Harpe, K.; Su, C.; Law, Y.K.; Crespo-Hernández, C.E.; Kohler, B. DNA Excited-State Dynamics: From Single Bases to the Double Helix. *Annu. Rev. Phys. Chem.* **2009**, *60*, 217–239. [CrossRef]
10. Ullrich, S.; Schultz, T.; Zgierski, M.Z.; Stolow, A. Electronic relaxation dynamics in DNA and RNA bases studied by time-resolved photoelectron spectroscopy. *Phys. Chem. Chem. Phys.* **2004**, *6*, 2796–2801. [CrossRef]
11. Improta, R.; Santoro, F.; Blancafort, L. Quantum Mechanical Studies on the Photophysics and the Photochemistry of Nucleic Acids and Nucleobases. *Chem. Rev.* **2016**, *116*, 3540–3593. [CrossRef] [PubMed]
12. Karsili, T.N.V.; Marchetti, B.; Ashfold, M.N.R.; Domcke, W. Ab initio study of potential ultrafast internal conversion routes in oxybenzone, caffeic acid, and ferulic acid: Implications for sunscreens. *J. Phys. Chem. A* **2014**, *118*, 11999–12010. [CrossRef]
13. Baker, L.A.; Marchetti, B.; Karsili, T.N.V.; Stavros, V.G.; Ashfold, M.N.R. Photoprotection: Extending lessons learned from studying natural sunscreens to the design of artificial sunscreen constituents. *Chem. Soc. Rev.* **2017**, *46*, 3770–3791. [CrossRef]
14. Holt, E.L.; Stavros, V.G. Applications of ultrafast spectroscopy to sunscreen development, from first principles to complex mixtures. *Int. Rev. Phys. Chem.* **2019**, *38*, 243–285. [CrossRef]
15. Woolley, J.M.; Losantos, R.; Sampedro, D.; Stavros, V.G. Computational and experimental characterization of novel ultraviolet filters. *Phys. Chem. Chem. Phys.* **2020**, *22*, 25390–25395. [CrossRef] [PubMed]
16. Harris, S.J.; Karsili, T.N.V.; Murdock, D.; Oliver, T.A.A.; Wenge, A.M.; Zaouris, D.K.; Ashfold, M.N.R.; Harvey, J.N.; Few, J.D.; Gowrie, S.; et al. A Multipronged Comparative Study of the Ultraviolet Photochemistry of 2-, 3-, and 4-Chlorophenol in the Gas Phase. *J. Phys. Chem. A* **2015**, *119*, 6045–6056. [CrossRef] [PubMed]
17. Lin, Y.-C.; Lee, C.; Lee, S.-H.; Lee, Y.-Y.; Lee, Y.T.; Tseng, C.-M.; Ni, C.-K. Excited-state dissociation dynamics of phenol studied by a new time-resolved technique. *J. Chem. Phys.* **2018**, *148*, 74306. [CrossRef]
18. Nix, M.G.D.; Devine, A.L.; Cronin, B.; Dixon, R.N.; Ashfold, M.N.R. High resolution photofragment translational spectroscopy studies of the near ultraviolet photolysis of phenol. *J. Chem. Phys.* **2006**, *125*, 133318. [CrossRef]
19. Roberts, G.M.; Chatterley, A.S.; Young, J.D.; Stavros, V.G. Direct observation of hydrogen tunneling dynamics in photoexcited phenol. *J. Phys. Chem. Lett.* **2012**, *3*, 348–352. [CrossRef]
20. Iqbal, A.; Cheung, M.S.Y.; Nix, M.G.D.; Stavros, V.G. Exploring the time-scales of H-atom detachment from photoexcited phenol-h6 and phenol-d5: Statistical vs. Nonstatistical decay. *J. Phys. Chem. A* **2009**, *113*, 8157–8163. [CrossRef]
21. Ashfold, M.N.R.; Devine, A.L.; Dixon, R.N.; King, G.A.; Nix, M.G.D.; Oliver, T.A.A. Exploring nuclear motion through conical intersections in the UV photodissociation of phenols and thiophenol. *Proc. Natl. Acad. Sci. USA* **2008**, *105*, 12701–12706. [CrossRef]
22. Vieuxmaire, O.P.J.; Lan, Z.; Sobolewski, A.L.; Domcke, W. Ab initio characterization of the conical intersections involved in the photochemistry of phenol. *J. Chem. Phys.* **2008**, *129*, 224307. [CrossRef] [PubMed]
23. Karsili, T.N.V.; Wenge, A.M.; Harris, S.J.; Murdock, D.; Harvey, J.N.; Dixon, R.N.; Ashfold, M.N.R. O-H bond fission in 4-substituted phenols: S_1 state predissociation viewed in a Hammett-like framework. *Chem. Sci.* **2013**, *4*, 2434–2446. [CrossRef]
24. Iqbal, A.; Pegg, L.J.; Stavros, V.G. Direct versus indirect H atom elimination from photoexcited phenol molecules. *J. Phys. Chem. A* **2008**, *112*, 9531–9534. [CrossRef] [PubMed]
25. Karsili, T.N.V.; Wenge, A.M.; Marchetti, B.; Ashfold, M.N.R. Symmetry matters: Photodissociation dynamics of symmetrically versus asymmetrically substituted phenols. *Phys. Chem. Chem. Phys.* **2014**, *16*, 588–598. [CrossRef] [PubMed]
26. Karsili, T.N.V.; Marchetti, B.; Moca, R.; Ashfold, M.N.R. UV photodissociation of pyrroles: Symmetry and substituent effects. *J. Phys. Chem. A* **2013**, *117*, 12067–12074. [CrossRef]
27. Vallet, V.; Lan, Z.; Mahapatra, S.; Sobolewski, A.L.; Domcke, W. Photochemistry of pyrrole: Time-dependent quantum wave-packet description of the dynamics at the $^1\pi\sigma^*$-S_0 conical intersections. *J. Chem. Phys.* **2005**, *123*, 144307. [CrossRef] [PubMed]
28. Vallet, V.; Lan, Z.; Mahapatra, S.; Sobolewski, A.L.; Domcke, W. Time-dependent quantum wave-packet description of the $^1\pi\sigma^*$ photochemistry of pyrrole. *Faraday Discuss.* **2004**, *127*, 283–293. [CrossRef]
29. Roberts, G.M.; Williams, C.A.; Yu, H.; Chatterley, A.S.; Young, J.D.; Ullrich, S.; Stavros, V.G. Probing ultrafast dynamics in photoexcited pyrrole: Timescales for $^1\pi\sigma^*$ mediated H-atom elimination. *Faraday Discuss.* **2013**, *163*, 95–116. [CrossRef]
30. Sobolewski, A.L.; Domcke, W. Conical intersections induced by repulsive $^1\pi\sigma^*$ states in planar organic molecules: Malonaldehyde, pyrrole and chlorobenzene as photochemical model systems. *Chem. Phys.* **2000**, *259*, 181–191. [CrossRef]

31. Cronin, B.; Nix, M.G.D.; Qadiri, R.H.; Ashfold, M.N.R. High resolution photofragment translational spectroscopy studies of the near ultraviolet photolysis of pyrrole. *Phys. Chem. Chem. Phys.* **2004**, *6*, 5031–5041. [CrossRef]
32. Staniforth, M.; Young, J.D.; Cole, D.R.; Karsili, T.N.V.; Ashfold, M.N.R.; Stavros, V.G. Ultrafast excited-state dynamics of 2,4-dimethylpyrrole. *J. Phys. Chem. A* **2014**, *118*, 10909–10918. [CrossRef]
33. Cole-Filipiak, N.C.; Staniforth, M.; Rodrigues, N.D.N.; Peperstraete, Y.; Stavros, V.G. Ultrafast Dissociation Dynamics of 2-Ethylpyrrole. *J. Phys. Chem. A* **2017**, *121*, 969–976. [CrossRef]
34. Blank, D.A.; North, S.W.; Lee, Y.T. The ultraviolet photodissociation dynamics of pyrrole. *Chem. Phys.* **1994**, *187*, 35–47. [CrossRef]
35. Iqbal, A.; Stavros, V.G. Exploring the Time Scales of H-Atom Elimination from Photoexcited Indole. *J. Phys. Chem. A* **2010**, *114*, 68–72. [CrossRef]
36. Sobolewski, A.L.; Domcke, W. Ab initio investigations on the photophysics of indole. *Chem. Phys. Lett.* **1999**, *315*, 293–298. [CrossRef]
37. Nix, M.G.D.; Devine, A.L.; Cronin, B.; Ashfold, M.N.R. High resolution photofragment translational spectroscopy of the near UV photolysis of indole: Dissociation via the $^1\pi\sigma^*$ state. *Phys. Chem. Chem. Phys.* **2006**, *8*, 2610–2618. [CrossRef]
38. Lin, M.-F.; Tseng, C.-M.; Lee, Y.T.; Ni, C.-K. Photodissociation dynamics of indole in a molecular beam. *J. Chem. Phys.* **2005**, *123*, 124303. [CrossRef] [PubMed]
39. Matsika, S. Radiationless Decay of Excited States of Uracil through Conical Intersections. *J. Phys. Chem. A* **2004**, *108*, 7584–7590. [CrossRef]
40. Lan, Z.; Fabiano, E.; Thiel, W. Photoinduced Nonadiabatic Dynamics of 9H-Guanine. *ChemPhysChem* **2009**, *10*, 1225–1229. [CrossRef] [PubMed]
41. Kistler, K.A.; Matsika, S. Photophysical pathways of cytosine in aqueous solution. *Phys. Chem. Chem. Phys.* **2010**, *12*, 5024–5031. [CrossRef]
42. Delchev, V.B.; Sobolewski, A.L.; Domcke, W. Comparison of the non-radiative decay mechanisms of 4-pyrimidinone and uracil: An ab initio study. *Phys. Chem. Chem. Phys.* **2010**, *12*, 5007–5015. [CrossRef] [PubMed]
43. Barbatti, M.; Szymczak, J.J.; Aquino, A.J.A.; Nachtigallov, D.; Lischka, H. The decay mechanism of photoexcited guanine—A nonadiabatic dynamics study. *J. Chem. Phys.* **2011**, *134*, 14304. [CrossRef]
44. Nachtigallovaí, D.; Aquino, A.J.A.; Szymczak, J.J.; Barbatti, M.; Hobza, P.; Lischka, H. Nonadiabatic dynamics of uracil: Population split among different decay mechanisms. *J. Phys. Chem. A* **2011**, *115*, 5247–5255. [CrossRef]
45. Perun, S.; Sobolewski, A.L.; Domcke, W. Ab initio studies on the radiationless decay mechanisms of the lowest excited singlet states of 9H-adenine. *J. Am. Chem. Soc.* **2005**, *127*, 6257–6265. [CrossRef] [PubMed]
46. Serrano-Andrés, L.; Merchán, M.; Borin, A.C. A Three-State Model for the Photophysics of Adenine. *Chem. A Eur. J.* **2006**, *12*, 6559–6571. [CrossRef] [PubMed]
47. Barbatti, M.; Lischka, H. Nonadiabatic deactivation of 9H-adenine: A comprehensive picture based on mixed quantum-classical dynamics. *J. Am. Chem. Soc.* **2008**, *130*, 6831–6839. [CrossRef] [PubMed]
48. Conti, I.; Garavelli, M.; Orlandi, G. Deciphering low energy deactivation channels in adenine. *J. Am. Chem. Soc.* **2009**, *131*, 16108–16118. [CrossRef] [PubMed]
49. Barbatti, M.; Lan, Z.; Crespo-Otero, R.; Szymczak, J.J.; Lischka, H.; Thiel, W. Critical appraisal of excited state nonadiabatic dynamics simulations of 9H-adenine. *J. Chem. Phys.* **2012**, *137*, 22A503. [CrossRef] [PubMed]
50. Zgierski, M.Z.; Patchkovskii, S.; Fujiwara, T.; Lim, E.C. On the Origin of the Ultrafast Internal Conversion of Electronically Excited Pyrimidine Bases. *J. Phys. Chem. A* **2005**, *109*, 9384–9387. [CrossRef]
51. Triandafillou, C.G.; Matsika, S. Excited-state tautomerization of gas-phase cytosine. *J. Phys. Chem. A* **2013**, *117*, 12165–12174. [CrossRef]
52. Plasser, F.; Crespo-Otero, R.; Pederzoli, M.; Pittner, J.; Lischka, H.; Barbatti, M. Surface hopping dynamics with correlated single-reference methods: 9H-adenine as a case study. *J. Chem. Theory Comput.* **2014**, *10*, 1395–1405. [CrossRef]
53. Marian, C.M. The guanine tautomer puzzle: Quantum chemical investigation of ground and excited states. *J. Phys. Chem. A* **2007**, *111*, 1545–1553. [CrossRef] [PubMed]
54. Matsika, S.; Krause, P. Nonadiabatic events and conical intersections. *Ann. Rev. Phys. Chem.* **2011**, *62*, 621–643. [CrossRef] [PubMed]
55. Prokhorenko, V.I.; Picchiotti, A.; Pola, M.; Dijkstra, A.G.; Miller, R.J.D. New Insights into the Photophysics of DNA Nucleobases. *J. Phys. Chem. Lett.* **2016**, *7*, 4445–4450. [CrossRef] [PubMed]
56. Pepino, A.J.; Segarra-Martí, J.; Nenov, A.; Improta, R.; Garavelli, M. Resolving Ultrafast Photoinduced Deactivations in Water-Solvated Pyrimidine Nucleosides. *J. Phys. Chem. Lett.* **2017**, *8*, 1777–1783. [CrossRef]
57. Francés-Monerris, A.; Gattuso, H.; Roca-Sanjuán, D.; Tuñón, I.; Marazzi, M.; Dumont, E.; Monari, A. Dynamics of the excited-state hydrogen transfer in a (dG)·(dC) homopolymer: Intrinsic photostability of DNA. *Chem. Sci.* **2018**, *9*, 7902–7911. [CrossRef] [PubMed]
58. Pilles, B.M.; Maerz, B.; Chen, J.; Bucher, D.B.; Gilch, P.; Kohler, B.; Zinth, W.; Fingerhut, B.P.; Schreier, W.J. Decay Pathways of Thymine Revisited. *J. Phys. Chem. A* **2018**, *122*, 4819–4828. [CrossRef] [PubMed]
59. Perun, S.; Sobolewski, A.L.; Domcke, W. Conical Intersections in Thymine. *J. Phys. Chem. A* **2006**, *110*, 13238–13244. [CrossRef] [PubMed]
60. Ismail, N.; Blancafort, L.; Olivucci, M.; Kohler, B.; Robb, M.A. Ultrafast decay of electronically excited singlet cytosine via a π,π^* to n_0,π^* state switch. *J. Am. Chem. Soc.* **2002**, *124*, 6818–6819. [CrossRef]

61. Blancafort, L.; Cohen, B.; Hare, P.M.; Kohler, B.; Robb, M.A. Singlet excited-state dynamics of 5-fluorocytosine and cytosine: An experimental and computational study. *J. Phys. Chem. A* **2005**, *109*, 4431–4436. [CrossRef]
62. Kistler, K.A.; Matsika, S. Radiationless decay mechanism of cytosine: An ab initio study with comparisons to the fluorescent analogue 5-methyl-2-pyrimidinone. *J. Phys. Chem. A* **2007**, *111*, 2650–2661. [CrossRef]
63. Zechmann, G.; Barbatti, M. Photophysics and deactivation pathways of thymine. *J. Phys. Chem. A* **2008**, *112*, 8273–8279. [CrossRef] [PubMed]
64. Asturiol, D.; Lasorne, B.; Robb, M.A.; Blancafort, L. Photophysics of the π,π and n,π states of thymine: MS-CASPT2 minimum-energy paths and CASSCF on-the-fly dynamics. *J. Phys. Chem. A* **2009**, *113*, 10211–10218. [CrossRef]
65. Yamazaki, S.; Domcke, W.; Sobolewski, A.L. Nonradiative Decay Mechanisms of the Biologically Relevant Tautomer of Guanine. *J. Phys. Chem. A* **2008**, *112*, 11965–11968. [CrossRef] [PubMed]
66. Domcke, W.; Yarkony, D.R.; Koeppel, H. *Conical Intersections: Theory, Computation and Experiment*; World Scientific: Singapore, 2011.
67. Domcke, W.; Yarkony, D.R.; Koeppel, H. *Conical Intersections: Electronic Structure, Dynamics & Spectroscopy*; World Scientific: Singapore, 2004.
68. Baker, L.A.; Horbury, M.D.; Greenough, S.E.; Ashfold, M.N.R.; Stavros, V.G. Broadband Ultrafast Photoprotection by Oxybenzone Across the UVB and UVC Spectral Regions. *Photochem. Photobiol. Sci.* **2015**, *14*, 1814–1820. [CrossRef] [PubMed]
69. Baker, L.A.; Horbury, M.D.; Greenough, S.E.; Coulter, P.M.; Karsili, T.N.V.; Roberts, G.M.; Orr-Ewing, A.J.; Ashfold, M.N.R.; Stavros, V.G. Probing the Ultrafast Energy Dissipation Mechanism of the Sunscreen Oxybenzone after UVA Irradiation. *J. Phys. Chem. Lett.* **2015**, *6*, 1363–1368. [CrossRef] [PubMed]
70. Baker, L.A.; Grosvenor, L.C.; Ashfold, M.N.R.; Stavros, V.G. Ultrafast Photophysical Studies of a Multicomponent Sunscreen: Oxybenzone—Titanium Dioxide Mixtures. *Chem. Phys. Lett.* **2016**, *664*, 39–43. [CrossRef]
71. Deng, Z.; Sun, S.; Zhou, M.; Huang, G.; Pang, J.; Dang, L.; Li, M.-D. Revealing Ultrafast Energy Dissipation Pathway of Nanocrystalline Sunscreens Oxybenzone and Dioxybenzone. *J. Phys. Chem. Lett.* **2019**, *10*, 6499–6503. [CrossRef]
72. Li, C.-X.; Guo, W.-W.; Xie, B.-B.; Cui, G. Photodynamics of oxybenzone sunscreen: Nonadiabatic dynamics simulations. *J. Chem. Phys.* **2016**, *145*, 74308. [CrossRef] [PubMed]
73. McGrath, J.A.; Eady, R.A.J.; Pope, F.M. *Rook's Textb. Dermatology*; John Wiley & Sons: Hoboken, NJ, USA, 2004.
74. Solano, F. Photoprotection and skin pigmentation: Melanin-related molecules and some other new agents obtained from natural sources. *Molecules* **2020**, *25*, 1537. [CrossRef] [PubMed]
75. Sobolewski, A.L.; Domcke, W. Photophysics of eumelanin: Ab initio studies on the electronic spectroscopy and photochemistry of 5,6-dihydroxyindole. *Chemphyschem* **2007**, *8*, 756–762. [CrossRef] [PubMed]
76. Corani, A.; Huijser, A.; Iadonisi, A.; Pezzella, A.; Sundström, V.; d'Ischia, M. Bottom-Up Approach to Eumelanin Photoprotection: Emission Dynamics in Parallel Sets of Water-Soluble 5,6-Dihydroxyindole-Based Model Systems. *J. Phys. Chem. B* **2012**, *116*, 13151–13158. [CrossRef] [PubMed]
77. Corani, A.; Huijser, A.; Gustavsson, T.; Markovitsi, D.; Malmqvist, P.-Å.; Pezzella, A.; d'Ischia, M.; Sundström, V. Superior Photoprotective Motifs and Mechanisms in Eumelanins Uncovered. *J. Am. Chem. Soc.* **2014**, *136*, 11626–11635. [CrossRef] [PubMed]
78. Marchetti, B.; Karsili, T.N.V. Theoretical insights into the photo-protective mechanisms of natural biological sunscreens: Building blocks of eumelanin and pheomelanin. *Phys. Chem. Chem. Phys.* **2016**, *18*, 3644–3658. [CrossRef] [PubMed]
79. Datar, A.; Hazra, A. Pathways for Excited-State Nonradiative Decay of 5,6-Dihydroxyindole, a Building Block of Eumelanin. *J. Phys. Chem. A* **2017**, *121*, 2790–2797. [CrossRef] [PubMed]
80. Ghosh, P.; Ghosh, D. Non-radiative decay of an eumelanin monomer: To be or not to be planar. *Phys. Chem. Chem. Phys.* **2019**, *21*, 6635–6642. [CrossRef] [PubMed]
81. Ghosh, P.; Ghosh, D. Effect of microsolvation on the non-radiative decay of the eumelanin monomer. *Phys. Chem. Chem. Phys.* **2019**, *21*, 26123–26132. [CrossRef] [PubMed]
82. Crane, S.W.; Ghafur, O.; Cowie, T.Y.; Lindsay, A.G.; Thompson, J.O.F.; Greenwood, J.B.; Bebbington, M.W.P.; Townsend, D. Dynamics of electronically excited states in the eumelanin building block 5,6-dihydroxyindole. *Phys. Chem. Chem. Phys.* **2019**, *21*, 8152–8160. [CrossRef]
83. Gauden, M.; Pezzella, A.; Panzella, L.; Napolitano, A.; d'Ischia, M.; Sundström, V. Ultrafast Excited State Dynamics of 5,6-Dihydroxyindole, A Key Eumelanin Building Block: Nonradiative Decay Mechanism. *J. Phys. Chem. B* **2009**, *113*, 12575–12580. [CrossRef] [PubMed]
84. Huijser, A.; Pezzella, A.; Hannestad, J.K.; Panzella, L.; Napolitano, A.; d'Ischia, M.; Sundström, V. UV-dissipation mechanisms in the eumelanin building block DHICA. *Chemphyschem* **2010**, *11*, 2424–2431. [CrossRef]
85. Corani, A.; Pezzella, A.; Pascher, T.; Gustavsson, T.; Markovitsi, D.; Huijser, A.; d'Ischia, M.; Sundström, V. Excited-State Proton-Transfer Processes of DHICA Resolved: From Sub-Picoseconds to Nanoseconds. *J. Phys. Chem. Lett.* **2013**, *4*, 1383–1388. [CrossRef] [PubMed]
86. Oliver, T.A.A.; King, G.A.; Ashfold, M.N.R. Position matters: Competing O–H and N–H photodissociation pathways in hydroxy- and methoxy-substituted indoles. *Phys. Chem. Chem. Phys.* **2011**, *13*, 14646–14662. [CrossRef] [PubMed]
87. Crane, S.W.; Ghafur, O.; Saalbach, L.; Paterson, M.J.; Townsend, D. The influence of substituent position on the excited state dynamics operating in 4-, 5- and 6-hydroxyindole. *Chem. Phys. Lett.* **2020**, *738*, 136870. [CrossRef]

88. King, G.A.; Oliver, T.A.A.; Dixon, R.N.; Ashfold, M.N.R. Vibrational energy redistribution in catechol during ultraviolet photolysis. *Phys. Chem. Chem. Phys.* **2012**, *14*, 3338–3345. [CrossRef]
89. Chatterley, A.S.; Young, J.D.; Townsend, D.; Żurek, J.M.; Paterson, M.J.; Roberts, G.M.; Stavros, V.G. Manipulating dynamics with chemical structure: Probing vibrationally-enhanced tunnelling in photoexcited catechol. *Phys. Chem. Chem. Phys.* **2013**, *15*, 6879–6892. [CrossRef]
90. Young, J.D.; Staniforth, M.; Paterson, M.J.; Stavros, V.G. Torsional Motion of the Chromophore Catechol following the Absorption of Ultraviolet Light. *Phys. Rev. Lett.* **2015**, *114*, 233001. [CrossRef] [PubMed]
91. Grieco, C.; Kohl, F.R.; Zhang, Y.; Natarajan, S.; Blancafort, L.; Kohler, B. Intermolecular Hydrogen Bonding Modulates O-H Photodissociation in Molecular Aggregates of a Catechol Derivative. *Photochem. Photobiol.* **2019**, *95*, 163–175. [CrossRef] [PubMed]
92. Grieco, C.; Hanes, A.T.; Blancafort, L.; Kohler, B. Effects of Intra- and Intermolecular Hydrogen Bonding on O-H Bond Photodissociation Pathways of a Catechol Derivative. *J. Phys. Chem. A* **2019**, *123*, 5356–5366. [CrossRef]
93. Turner, M.A.P.; Turner, R.J.; Horbury, M.D.; Hine, N.D.M.; Stavros, V.G. Examining solvent effects on the ultrafast dynamics of catechol. *J. Chem. Phys.* **2019**, *151*, 84305. [CrossRef]
94. Anh, N.V.; Williams, R.M. Bis-semiquinone (bi-radical) formation by photoinduced proton coupled electron transfer in covalently linked catechol–quinone systems: Aviram's hemiquinones revisited. *Photochem. Photobiol. Sci.* **2012**, *11*, 957–961. [CrossRef] [PubMed]
95. Grieco, C.; Empey, J.M.; Kohl, F.R.; Kohler, B. Probing eumelanin photoprotection using a catechol:quinone heterodimer model system. *Faraday Discuss.* **2019**, *216*, 520–537. [CrossRef]
96. Mardirossian, N.; Head-Gordon, M. ωb97X-D: A 10-parameter, range-separated hybrid, generalized gradient approximation density functional with nonlocal correlation, designed by a survival-of-the-fittest strategy. *Phys. Chem. Chem. Phys.* **2014**, *16*, 9904–9924. [CrossRef]
97. Hehre, W.J.; Stewart, R.F.; Pople, J.A. Self-Consistent Molecular-Orbital Methods. I. Use of Gaussian Expansions of Slater-Type Atomic Orbitals. *J. Chem. Phys.* **1969**, *51*, 2657–2664. [CrossRef]
98. Léger, S.J.; Marchetti, B.; Ashfold, M.N.R.; Karsili, T.N.V. The Role of Norrish Type-I Chemistry in Photoactive Drugs: An ab initio Study of a Cyclopropenone-Enediyne Drug Precursor. *Front. Chem.* **2020**, *8*, 1200. [CrossRef]
99. Andersson, K.; Malmqvist, P.; Roos, B.O. Second-order perturbation theory with a complete active space self-consistent field reference function. *J. Chem. Phys.* **1992**, *96*, 1218–1226. [CrossRef]
100. Frisch, M.J.; Trucks, G.W.; Schlegel, H.B.; Scuseria, G.E.; Robb, M.A.; Cheeseman, J.R.; Scalmani, G.; Barone, V.; Petersson, G.A.; Nakatsuji, H.; et al. *Gaussian 16, Revision C.01*; Gaussian Inc.: Wallingford, CT, USA, 2016.
101. Werner, H.-J.; Knowles, P.J.; Knizia, G.; Manby, F.R.; Schütz, M. Molpro: A general-purpose quantum chemistry program package. *WIREs Comput. Mol. Sci.* **2012**, *2*, 242–253. [CrossRef]
102. Banyasz, A.; Ketola, T.; Martinez-Fernandez, L.; Improta, R.; Markovitsi, D. Adenine radicals generated in alternating AT duplexes by direct absorption of low-energy UV radiation. *Faraday Discuss.* **2018**, *207*, 181–197. [CrossRef] [PubMed]
103. Perun, S.; Sobolewski, A.L.; Domcke, W. Role of electron-driven proton-transfer processes in the excited-state deactivation of the adenine-thymine base pair. *J. Phys. Chem. A* **2006**, *110*, 9031–9038. [CrossRef]
104. Nogueira, J.J.; Corani, A.; el Nahhas, A.; Pezzella, A.; d'Ischia, M.; González, L.; Sundström, V. Sequential Proton-Coupled Electron Transfer Mediates Excited-State Deactivation of a Eumelanin Building Block. *J. Phys. Chem. Lett.* **2017**, *8*, 1004–1008. [CrossRef]
105. Sobolewski, A.L.; Domcke, W.; Hättig, C. Tautomeric selectivity of the excited-state lifetime of guanine/cytosine base pairs: The role of electron-driven proton-transfer processes. *Proc. Natl. Acad. Sci. USA* **2005**, *102*, 17903–17906. [CrossRef] [PubMed]
106. Gobbo, J.P.; Saurí, V.; Roca-Sanjuán, D.; Serrano-Andrés, L.; Merchán, M.; Borin, A.C. On the Deactivation Mechanisms of Adenine–Thymine Base Pair. *J. Phys. Chem. B* **2012**, *116*, 4089–4097. [CrossRef] [PubMed]
107. Groenhof, G.; Schäfer, L.V.; Boggio-Pasqua, M.; Goette, M.; Grubmüller, H.; Robb, M.A. Ultrafast Deactivation of an Excited Cytosine−Guanine Base Pair in DNA. *J. Am. Chem. Soc.* **2007**, *129*, 6812–6819. [CrossRef] [PubMed]
108. Sauri, V.; Gobbo, J.P.; Serrano-Pérez, J.J.; Lundberg, M.; Coto, P.B.; Serrano-Andrés, L.; Borin, A.C.; Lindh, R.; Merchán, M.; Roca-Sanjuán, D. Proton/Hydrogen Transfer Mechanisms in the Guanine–Cytosine Base Pair: Photostability and Tautomerism. *J. Chem. Theory Comput.* **2013**, *9*, 481–496. [CrossRef] [PubMed]
109. Röttger, K.; Marroux, H.J.B.; Grubb, M.P.; Coulter, P.M.; Böhnke, H.; Henderson, A.S.; Galan, M.C.; Temps, F.; Orr-Ewing, A.J.; Roberts, G.M. Ultraviolet Absorption Induces Hydrogen-Atom Transfer in G·C Watson–Crick DNA Base Pairs in Solution. *Angew. Chemie Int. Ed.* **2015**, *54*, 14719–14722. [CrossRef]
110. Crespo-Hernández, C.E.; Cohen, B.; Kohler, B. Base stacking controls excited-state dynamics in A·T DNA. *Nature* **2005**, *436*, 1141–1144. [CrossRef]
111. Zhang, Y.; de la Harpe, K.; Beckstead, A.A.; Improta, R.; Kohler, B. UV-Induced Proton Transfer between DNA Strands. *J. Am. Chem. Soc.* **2015**, *137*, 7059–7062. [CrossRef]